

# THE MISMEASURE OF MERGERS: REVISED LIMITS ON SELF-INTERACTING DARK MATTER IN MERGING GALAXY CLUSTERS

DAVID WITTMAN<sup>1,2</sup>, NATHAN GOLOVICH<sup>1</sup>, WILLIAM A. DAWSON<sup>3</sup>  
*Draft version December 13, 2018*

## ABSTRACT

In an influential recent paper, Harvey et al. (2015) derive an upper limit to the self-interaction cross section of dark matter ( $\sigma_{\text{DM}}/m < 0.47 \text{ cm}^2/\text{g}$  at 95% confidence) by averaging the dark matter-galaxy offsets in a sample of merging galaxy clusters. Using much more comprehensive data on the same clusters, we identify several substantial errors in their offset measurements. Correcting these errors relaxes the upper limit on  $\sigma_{\text{DM}}/m$  to  $\lesssim 2 \text{ cm}^2/\text{g}$ , following the Harvey et al. (2015) prescription for relating offsets to cross sections in a simple solid body scattering model. Furthermore, many clusters in the sample violate the assumptions behind this prescription, so even this revised upper limit should be used with caution. Although this particular sample does not tightly constrain self-interacting dark matter models when analyzed this way, we discuss how merger ensembles may be used more effectively in the future. We conclude that errors inherent in using single-band imaging to identify mass and light peaks do not necessarily average out in a sample of this size, particularly when a handful of substructures constitute a majority of the weight in the ensemble.

## 1. INTRODUCTION

Dark matter (DM) comprises most of the matter in the universe but little is known about its properties. It has been detected gravitationally, but despite many searches there is as yet no evidence it participates in other known interactions. Perhaps the dominant DM particle model has been the weakly interacting massive particle (WIMP), which is difficult to detect directly. Searches for weak interactions of dark matter with normal matter have rapidly improved in sensitivity, however, and are beginning to rule out interestingly large regions of parameter space (see Klasen et al. 2015, for a review). Another class of models, hidden sector models, posit substantial interactions *between* DM particles even if nongravitational interactions with normal matter are undetectably weak or nonexistent (Feldman et al. 2007; Feng & Kumar 2008; Cohen et al. 2010). Empirical constraints on DM self-interactions rely on astrophysical arguments and are much less stringent than those on interactions between DM and normal matter. Upper limits from astrophysical arguments (e.g., Randall et al. 2008) are on the order of one  $\text{cm}^2/\text{g}$ , or two barns per GeV—twenty orders of magnitude larger than the cross-sections relevant to collider and direct-detection searches.<sup>4</sup>

In other words, if DM particles interact with each other with about the same cross section as neutrons do, this interaction could still have escaped detection to date. This has provided general motivation for efforts to tighten astrophysical constraints on  $\sigma_{\text{DM}}/m$ . A more specific motivation comes from measurements of dwarf galaxy and

galaxy cluster density profiles, which are suggestive of self-interacting DM (SIDM) with a cross section around  $0.1\text{--}5 \text{ cm}^2/\text{g}$  (Boylan-Kolchin et al. 2012; Rocha et al. 2013; Peter et al. 2013; Sand et al. 2008; Newman et al. 2013b,a; Elbert et al. 2015). If true, this would exclude the WIMP model by some twenty orders of magnitude and point the way to some truly new physics. Skeptics, however, point out that these astrophysical environments also contain difficult-to-model baryonic effects that could explain the measured profiles (e.g. Brooks 2014).

A complementary method for probing some types of self-interactions may be to analyze mergers of galaxy clusters (which are mostly DM by mass) as “dark matter colliders.” The well-known Bullet Cluster serves as the best example and yields, at 68% confidence,  $\sigma_{\text{DM}}/m < 0.7 \text{ cm}^2/\text{g}$  based on a mass-to-light argument and  $\sigma_{\text{DM}}/m < 1.25 \text{ cm}^2/\text{g}$  based on the offset argument described in more detail below (Randall et al. 2008). An ensemble of such mergers could potentially drive this upper limit down enough to confirm SIDM if it exists. Because cluster mergers and galaxy cores probe different velocity scales, such a detection would also characterize the velocity dependence of the interaction and thereby constrain the mediator mass (Loeb & Weiner 2011; Zavala et al. 2013; Kaplinghat et al. 2016). Even if one prefers to view this work as an exercise in excluding SIDM, observations on both low and high velocity scales will be necessary to impinge on the broad class of SIDM models that are naturally velocity dependent (Loeb & Weiner 2011).

Hence there is great interest in the result of Harvey et al. (2015, hereafter H15), who used offsets between galaxies and DM in an ensemble of 30 merging clusters to derive, for a simple solid body scattering model, an upper limit of  $\sigma_{\text{DM}}/m < 0.47 \text{ cm}^2/\text{g}$  at 95% confidence and  $< -0.01 \text{ cm}^2/\text{g}$  at 68% confidence.<sup>5</sup> This is a dramatic improvement on the previous best constraint from

<sup>1</sup> Physics Department, University of California, Davis, CA 95616; dwittman@physics.ucdavis.edu

<sup>2</sup> Instituto de Astrofísica e Ciências do Espaço, Universidade de Lisboa, Lisbon, Portugal

<sup>3</sup> Lawrence Livermore National Laboratory, P.O. Box 808 L-210, Livermore, CA, 94551, USA

<sup>4</sup> DM cross sections are cited in terms of area per unit mass because the rather than area per particle because astronomers are able to measure the total mass of a collection of DM particles but not the mass per particle.

<sup>5</sup> The 68% confidence upper limit is not stated directly by H15 but is implied by their Figure 4.

offsets cited above, and thus has already helped drive new constraints on the velocity dependence and therefore the mediator mass (Kaplinghat et al. 2016). Because this dramatic improvement has profound implications for particle models, it warrants further scrutiny. Many of the merging clusters in the H15 sample have been intensively studied individually, thus providing independent measurements of numerous DM-galaxy offsets. These independent measurements derive from heterogeneous data sources and analysis methods, but always involve *more* data and analysis than H15 applied to any individual cluster. In this paper we use the more extensive data to reveal substantial errors that, when corrected, greatly loosen the H15 constraint.

The remainder of the paper is organized as follows. Section 2 reviews the basic premise behind the merging cluster technique and outlines the H15 procedure in enough detail to understand which substructures are most highly weighted in the final result. In Section 3 we review the literature on these highly-weighted substructures and either accept the H15 measurement, improve the H15 measurement, or argue that the substructure is unusable for this test. In Section 4 we analyze the updated catalog using the H15 formalism and derive updated SIDM constraints. In Section 5 we discuss the result in the broader context of astrophysical tests of dark matter, and present some concluding remarks.

## 2. THE MERGING CLUSTER TECHNIQUE

A galaxy cluster consists of gas, DM (constituting the great majority of the mass), and galaxies. When two such clusters fall together, the two sets of galaxies pass through each other with little or no exchange of momentum. The gas clouds, in contrast, exchange momentum and thereby slow down compared to the galaxies. A snapshot of a system soon after pericenter passage, for example the well-known Bullet Cluster, shows the two gas clouds closer to the center of the combined system and the galaxies farther out. The (at least approximately) collisionless nature of dark matter is then demonstrated when gravitational lensing shows that the majority of the mass (and by implication the DM) is coincident with the galaxies rather than the gas (Markevitch et al. 2004). If DM in fact exchanges some momentum in a way analogous to the gas, the DM at this stage of the merger will be located between the galaxies and the gas (Figure 1). The observed DM location thus constrains the DM self-interaction cross-section  $\sigma_{\text{DM}}/m$  in this model.<sup>6</sup>

The same reasoning applies to infall of smaller structures. In the limit of small structures falling into a much more massive structure, Harvey et al. (2014) developed an analytical relation between  $\sigma_{\text{DM}}/m$  and the galaxy-DM-gas geometry. Defining the galaxy-gas separation as  $\delta_{SG}$  ( $S$  stands for “star” which is synonymous with “galaxy” in this context), they define a coordinate system starting at the galaxy location and stretching to the gas location. The key observable is the DM displacement along this coordinate system,  $\delta_{SI}$ , in units of  $\delta_{SG}$ . This ratio,  $\frac{\delta_{SI}}{\delta_{SG}} \equiv \beta$ , has a simple analytical relationship to  $\sigma_{\text{DM}}/m$  if DM behaves analogously to the gas (see, how-

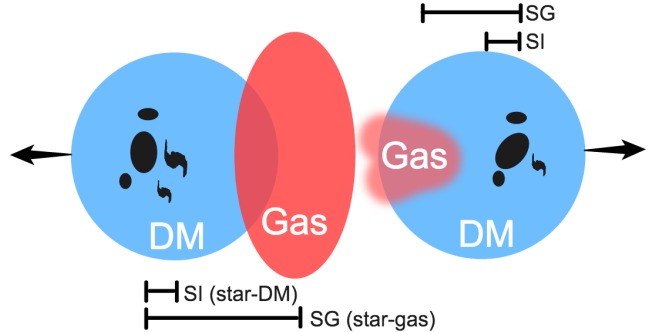


FIG. 1.— Schematic merger scenario: two subclusters have passed through each other, and the gas associated with each has slowed due to momentum exchange. This is observable as an offset between the star (i.e., galaxy) and gas positions,  $\delta_{SG}$ . In analogy, any star-DM offset  $\delta_{SI}$  may be attributed to momentum transfer between the DM halos and thus related to a cross section  $\sigma_{\text{DM}}/m$ . Subcluster masses and gas densities may vary considerably.

ever, Section 5 for caveats on this analogy).  $\beta = 0$  corresponds to collisionless DM,  $\beta = 1$  to DM just like baryonic gas, and intermediate values correspond to intermediate cross-sections. H15 averaged over 72 substructures and found  $\langle \beta \rangle = -0.04 \pm 0.07$ ; negative values are unphysical but indicate that the data are in tension with the idea of momentum transfer between the DM halos.

H15 analyzed 72 substructures in 30 systems. To identify the substructures with greatest influence on the ensemble result, note that standard propagation of errors on the ratio  $\beta \equiv \frac{\delta_{SI}}{\delta_{SG}}$  yields

$$\sigma_{\beta}^2 = \frac{\sigma_{SI}^2}{\delta_{SG}^2} + \frac{\sigma_{SG}^2 \delta_{SI}^2}{\delta_{SG}^4} \quad (1)$$

H15 adopt an uncertainty of  $\sigma_{SG} = \sigma_{SI} = 60$  kpc on each offset measurement. Therefore we can factor this out and write

$$\sigma_{\beta}^2 \propto \frac{1}{\delta_{SG}^2} \left( 1 + \frac{\delta_{SI}^2}{\delta_{SG}^2} \right). \quad (2)$$

With inverse-variance weighting, then, the weight of the  $i$ th substructure would be

$$w_i \propto \frac{\delta_{SG,i}^2}{1 + \delta_{SI,i}^2 / \delta_{SG,i}^2}. \quad (3)$$

Because  $\delta_{SI,i}^2 / \delta_{SG,i}^2 \ll 1$  in most cases,  $w_i \propto \delta_{SG,i}^2$  is a good approximation for quick assessment of the importance of a particular substructure in the ensemble. Although H15 multiply Gaussian probability density functions (PDFs) rather than compute a single inverse-variance weighted mean, the effect is the same: substructures with large  $\delta_{SG,i}$  predominantly determine the result. This makes intuitive sense, because the ratio  $\beta \equiv \frac{\delta_{SI}}{\delta_{SG}}$  is highly uncertain when the denominator is small compared to its 60 kpc uncertainty. Conversely, a large  $\delta_{SG,i}$  provides a stable baseline from which to measure the  $i$ th ratio, and this results in a narrow PDF, or effectively a large weight for the  $i$ th substructure.

Of course, one may question the adoption of  $\sigma_{SG} = \sigma_{SI} = 60$  kpc for each offset measurement, because the accuracy of offset measurements may vary substantially from substructure to substructure. Our immediate goal is to identify the substructures with the most influence

<sup>6</sup> Other self-interaction models are not well probed by the DM offset but may be probed with other observations; see Section 5.

on the H15 result, so we defer discussion of this point to Section 5.

Table 1 in Section 3.11 lists, in decreasing order, the weight of each substructure as a percentage of the total weight. The list is truncated after 16 substructures comprising 85% of the total weight. Next, we perform a literature review of these 16 substructures in descending order of weight.

### 3. LITERATURE REVIEW

We believe this paper will be most useful to the community if it highlights a handful of substantial inaccuracies in H15, rather than revisiting every detail. The following review thus defaults to respecting each H15 measurement unless the literature provides strong evidence to the contrary. Given the heterogeneity of the data, what constitutes “strong evidence” may vary. While acknowledging that this approach could lead to bias (discussed further in Section 5), we are confident that readers will agree with our corrections in most cases. In addition to outright corrections, we will discard substructures for which the matching between gas, DM, and galaxy components is uncertain (e.g., Subsection 3.1). In principle, one may choose instead to model such cases; heavy tails could reflect the probability that the given gas, DM, and galaxy components were never coincident in the past. However, quantifying this probability would be very difficult. Furthermore, we suspect that substructures with such heavy-tailed PDFs would contribute very little to an ensemble constraint. We therefore simply discard such cases.

Throughout this review, keep in mind that H15 used only single-band imaging (not necessarily the same band for each cluster) in their main analysis in order to yield a large and (in some respects) homogeneous sample. Multiband data allow for better selection of lensing sources and better exclusion of foreground galaxies when mapping the light distribution. Multiband imaging and spectra are also necessary to support a strong lensing analysis, which can locate the mass much more precisely than a weak lensing analysis. In fact, each of the highly weighted systems identified in Table 1 has been studied in more detail with some combination of these techniques. The bands observed, the availability of spectroscopy and strong lensing information, and the data processing and analysis choices vary. Nevertheless, we believe it would be wrong to ignore studies that employ far more data and more robust methods than H15 do on the very same merging systems.

Despite the heterogeneity, a few general remarks do apply. First, we do not seek to update the gas positions, because those are unaffected by the use of the additional data and techniques listed above. Of course X-ray analysis choices such as point source removal and smoothing scale are important, but this paper focuses on what can be learned from *additional data*. Second, we generally keep the nominal H15 uncertainty of 60 kpc on each offset, because the papers we draw from generally do not offer a detailed uncertainty analysis on these particular quantities. Third, lensing is sensitive to all forms of mass, not just DM, so the lensing position must be corrected for the gas mass contribution to obtain a position for the DM alone. Papers that supply more accurate lensing positions usually do not supply information necessary

to make this correction, so—except in cases where more specific information is available—we adopt the mean H15 correction of  $-4.3 \pm 1.6$  kpc (as a reminder, this is in a coordinate system originating at the galaxy position and increasing toward the gas position). The 1.6 kpc uncertainty in the mean of 72 substructures suggests a sample standard deviation of 13.6 kpc. For most substructures the nominal uncertainty in each offset is 60 kpc so the uncertainty in the gas mass correction is highly subdominant and will be neglected unless otherwise specified.

#### 3.1. Abell 2744 (Northwest)

The top panel of Figure 2 shows the H15 map of this cluster. To orient the reader, each H15 panel portrays one merging system, and each system has at least two substructures. Therefore, at least two independent offsets can be measured from each system (three in this case). In each H15 panel, the red contours indicate the surface brightness of the hot X-ray emitting gas, the green contours indicate galaxy brightness, and the blue contours indicate the mass (primarily DM) distribution as inferred from weak gravitational lensing. H15 draw a triangle connecting the peaks of the three distributions (gas, galaxies, mass) in each subcluster. If DM exhibits a drag force, we expect to find the mass peak between the galaxies and the gas, yielding  $\delta_{SI} > 0$ . This is referred to as DM “lagging” the galaxies because the gas definitely lags the galaxies (until turnaround; see Section 5). Lateral displacements are considered irrelevant—resulting from measurement error and perhaps other stochastic processes—so  $\delta_{SI}$  is actually the projection of the galaxy-DM leg of the triangle onto the galaxy-gas leg.

The length of the galaxy-gas leg,  $\delta_{SG}$ , determines the importance of the substructure in the ensemble analysis (§2); the top panel of Figure 2 shows that the northwest<sup>7</sup> substructure is by far the most important. This substructure is the most highly weighted in the entire ensemble, with 17% of the total weight, and we focus on it exclusively in this subsection. The corresponding H15 triangle appears to be a long line segment due to negligible lateral displacement. This triangle extends off the HST field of view because the Chandra X-ray Observatory, used to locate the gas, has a much larger field. The galaxy and DM components of this substructure are located on the edge of the HST field, with the DM trailing the galaxies, as predicted by the drag-force model if  $\sigma_{DM}/m > 0$ .

Merten et al. (2011) performed a detailed strong lensing, weak lensing and X-ray analysis of this cluster, imaging a larger area so the relevant substructure is no longer on the edge of the optical field (bottom panel of Figure 2). They supplemented two-band HST imaging with ground-based VLT and Subaru imaging, as well as 118 spectroscopic redshifts to guide the photometric selection of source galaxies for the lensing analysis. They resolved the western mass peak found by H15 into two distinct mass peaks (labeled NW1 and NW2 in the lower panel of Figure 2), separated by  $\sim 200$  kpc but on the *same* side of the gas. Merten et al. (2011) link both mass peaks to the gas peak via a complicated scenario far outside the Harvey et al. (2014) framework of an infalling subclus-

<sup>7</sup> H15 and this paper follow the astronomical convention of placing north up and east left on the page.

ter experiencing a small separation between its gas, DM, and galaxy components. Jauzac et al. (2016) developed a detailed strong-lensing mass model using additional data and confirmed the existence of NW1 and NW2, but found them to be coincident with their respective nearby bright galaxies. Meanwhile, Medezinski et al. (2016) analyzed Subaru and VLT imaging and derived quite different locations for the DM substructures in this system, as well as a different merger scenario. Given these complicated and competing merger scenarios, we cannot be certain that NW1 and/or NW2 were ever united with this particular gas peak. With the gas-galaxy-DM association itself in question, the offsets are not meaningful and the substructure should be omitted from the ensemble. In fact, Harvey et al. (2014) discussed association uncertainty and stated, correctly, that such uncertainty would vanish for substructures with offsets small enough to satisfy their approximation ( $< 30$  kpc). The association uncertainty arises here because  $\delta_{SG} \sim 400$  kpc, the largest in the H15 ensemble. Even if more robust associations can be made in the future, this substructure will never satisfy the Harvey et al. (2014) approximation.

Discarding this substructure should *strengthen* the H15 case against SIDM, because this is a very highly weighted substructure that—contrary to the H15 ensemble overall—does have a DM offset in the direction predicted by SIDM. It is worth noting, for illustration purposes only, that the configuration of green, blue, and red contours representing this substructure in the top panel of Figure 2 is to be expected if  $\sigma_{DM}/m \approx 1$  cm<sup>2</sup>/g. Specifically, for this cross section Equation 1 of H15, predicts  $\beta \equiv \frac{\delta_{SI}}{\delta_{SG}} = 0.14$ , while the (discarded) value here is 0.19. The substructures in H15 more typically exhibit green (galaxy) contours *between* the blue (DM) and red (gas) contours, corresponding to a negative  $\beta_i$  and a negative (unphysical) cross section.

In the remaining subsections of the literature review we will not comment on the impact of each particular correction to the H15 catalog; the foregoing explanation should enable the reader to do so if desired. For Abell 2744, we reiterate that omitting this substructure does nothing to loosen the constraints on  $\sigma_{DM}/m$ , quite the opposite in fact. Our final conclusion that the ensemble constraints are quite loose will owe nothing to the omission of this particular substructure.

### 3.2. DLSC J0916.2+2951 (South)

Dawson et al. (2012) and Dawson (2013) studied this cluster with two bands of HST/ACS imaging, five bands of deep ground-based imaging, and 634 spectroscopic redshifts to support the background source and galaxy member selection. Figure 3 compares the Dawson (2013) result with that of H15. The southern triangle in the top panel of Figure 3 illustrates the H15 finding that the mass is actually ahead of the galaxies; H15 found  $\delta_{SI} = -19$  kpc. The lower panel, from Dawson (2013), shows the lensing mass in a colorscale with galaxy luminosity density overlaid in white contours. The mass is clearly lagging the galaxies; Dawson (2013) found the offset to be +129 kpc based on the lensing peak alone, and +80 kpc after modeling out the gas mass to yield the DM mass alone.

While the H15 uncertainties are large enough to en-

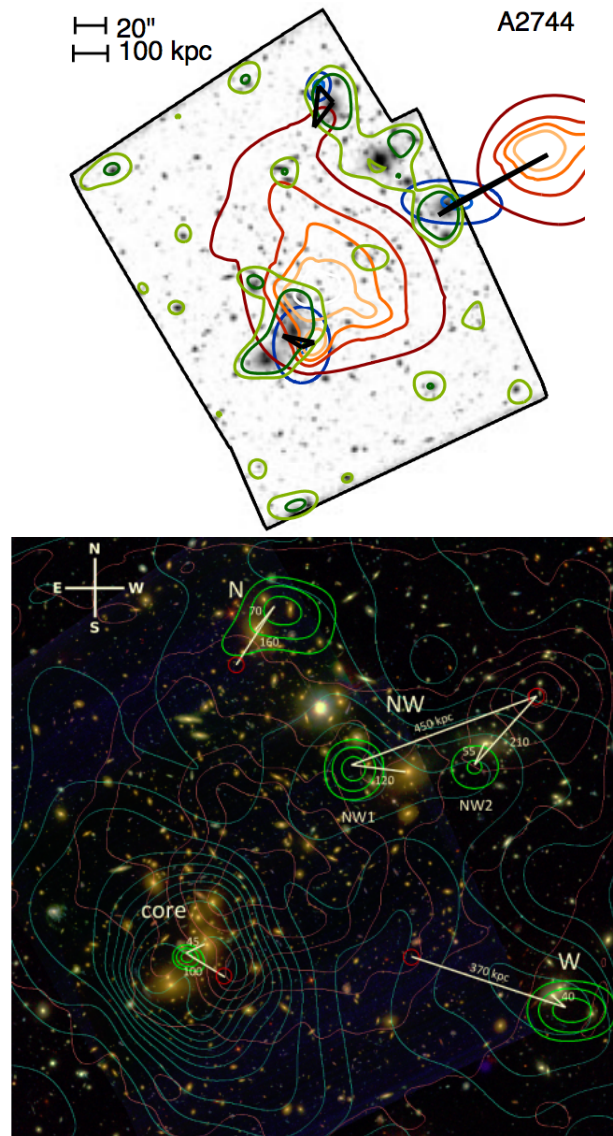


FIG. 2.— *Top*: View of Abell 2744 from H15. In all panels from H15, X-ray (gas) contours are reddish, green contours indicate visible light, and blue contours indicate mass inferred from gravitational lensing. In the highly weighted western subcluster the heavy black line indicates nearly collinear alignment of galaxies, DM and gas. *Bottom*: map from the more detailed analysis of Merten et al. (2011), with x-ray (red), lensing (cyan), and confidence contours for lensing peak locations (green, with  $0.3\sigma$ ,  $1\sigma$ ,  $2\sigma$  contours). The H15 mass peak is now resolved into two peaks (NW1 and NW2), contradicting the H15 assumption of simple infall of a gas-DM-galaxy substructure.

compass the Dawson (2013) value, the H15 mass position is outside the Dawson (2013)  $2\sigma$  confidence ellipse (the larger dashed ellipse). Because the Dawson (2013) value is supported by multiband selection of lensing sources and member galaxies, backed up by extensive spectroscopy, we adopt  $\delta_{SI} = 80$  kpc.

### 3.3. Abell 520

All five of the Abell 520 substructures identified by H15 are in the top 16 substructures by weight, so we review the entire system at once. In the top panel of Figure 4 we label the H15 substructures for reference below; the middle and bottom panels show multiband lensing analyses from Jee et al. (2014a) and Clowe et al. (2012) respec-

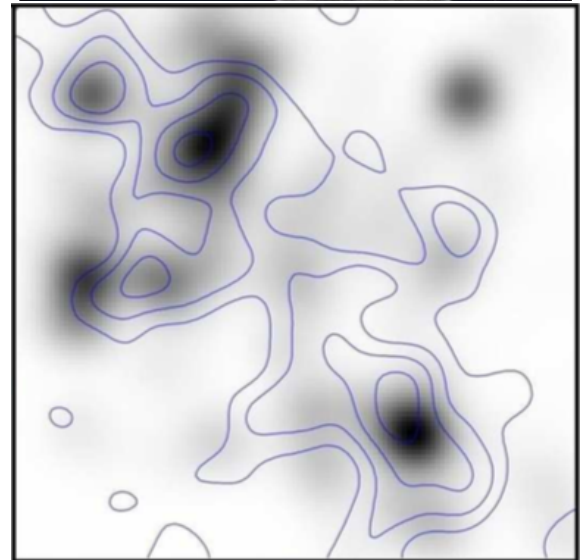
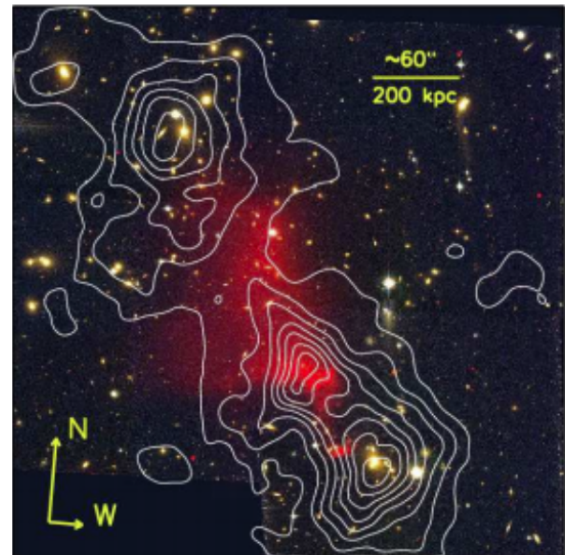
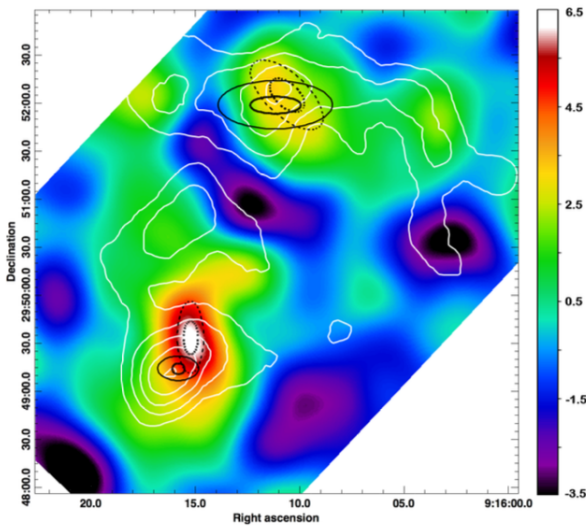
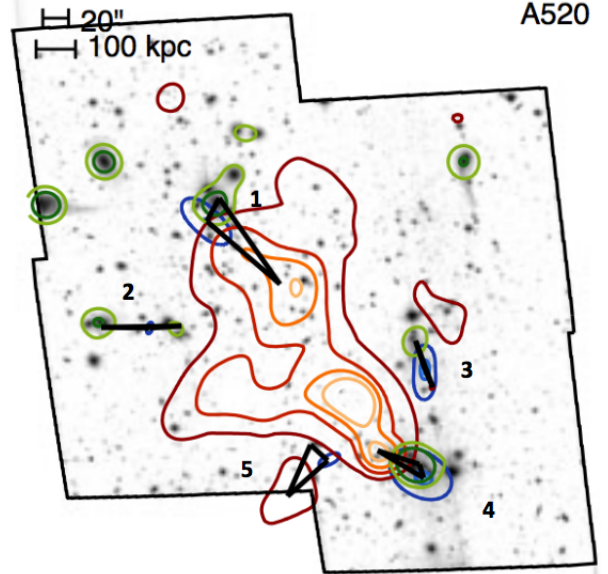
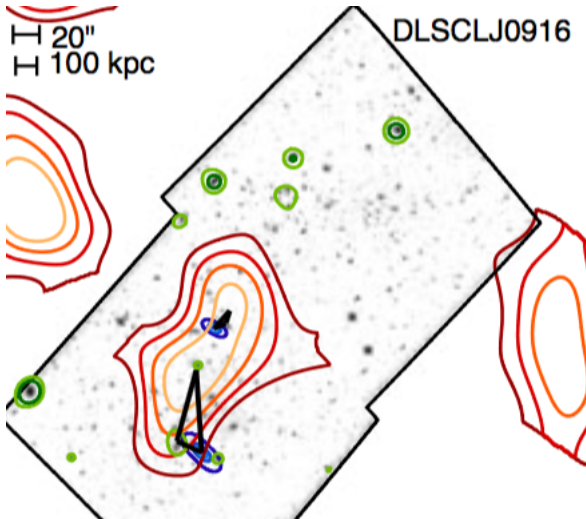


FIG. 3.— *Top*: View of DLSCL J0916 from H15. In the highly weighted southern subcluster, H15 find the mass to be ahead of the galaxies ( $\delta_{SI} = -19$  kpc), corresponding to a negative  $\sigma_{DM}/m$ . *Bottom*: the more detailed analysis of Dawson (2013), with mass in colorscale and galaxy luminosity density in white contours. In the south, the galaxy position agrees with that of H15 and thus serves as a reference point for comparing the two panels; Dawson (2013) find the mass to be trailing the galaxies. Solid (dashed) ellipses are 68% and 95% confidence intervals for the galaxy luminosity (mass) centroid.

tively. The latter two analyses broadly agree, with clear agreement on the main peaks (labeled 1 and 4 here) and both maps showing extensions toward the H15 peak labeled 5. The two maps agree weakly on the H15 peak we label 2, which appears as a peak in Clowe et al. (2012) but as a weaker extension of contours in Jee et al. (2014a). For our purposes, the major disagreement between the two detailed lensing analyses of Abell 520 is that Clowe et al. (2012) find a west-central peak, in the rough vicinity of H15 peak 3, while Jee et al. (2014a) does not.

*Substructure 1*: this northern subcluster is the most highly weighted of the five, with about 10% of the total weight of the H15 sample. This substructure is consistently identified and located by Jee et al. (2014a) and Clowe et al. (2012). Their maps qualitatively agree with H15, so we adopt the H15 offset.

FIG. 4.— *Top*: H15 analysis of Abell 520. The numerical labels are our annotation, to clearly link to descriptions of substructures in the text. *Middle*: multiband lensing analysis from Jee et al. (2014a), with X-ray in redscale and lensing contours in white. *Bottom*: multiband lensing analysis from Clowe et al. (2012) (contours) on top of smoothed galaxy light (grayscale).

*Substructure 2:* this is the second most highly weighted substructure in the system, with about 5% of the total weight of the H15 sample. However, there is no gas peak in the area. The absence of a gas peak prevents us from defining any gas-star-DM geometry. We therefore recommend omitting this putative substructure from the catalog.

We will see several more examples where the X-ray peak is not apparent in the H15 figure, so we address the issue more generally here. Presumably the gas peak in this substructure is not absent but merely at too low a signal-to-noise ratio (S/N) to appear on the H15 panel, which shows only a handful of contour levels. However, we see no indication of a diffuse X-ray source at this location in other presentations of the X-ray data, for example the pixelized redscale in the Jee et al. (2014a) panel, or the detailed X-ray analysis of this system presented by Markevitch et al. (2005). H15 automatically matched gas, galaxy, and DM peaks by searching for the nearest peak, so we suggest that this algorithm simply found a very low S/N local X-ray maximum. Many such local maxima must exist due to photon noise and unidentified point sources, but they should not be used to define substructures and offsets.

*Substructure 3:* the “gas peak” again appears to be a very low S/N local maximum with minimal angular extent. Furthermore, the H15 mass peak does not correspond to a peak in Jee et al. (2014a). Clowe et al. (2012) did find a center-west mass peak, but it lies 270 kpc from the H15 location, on the opposite side of a nearby set of galaxies. Finally, most of the light in the green H15 contour is actually a streak from the bright star to the north rather than galaxy light—this is more easily seen by comparison to the middle panel of Figure 4, which has fewer overlays. The streak is probably caused by some combination of CCD bleeding, charge transfer inefficiency, and the star being near the chip gap, which makes its effects on the neighboring chip more difficult to remove. The appearance of this streak thus varies greatly depending on the specifics of the image processing, for example it is absent in most press release images. Note also that Clowe et al. (2012) used color information to select member galaxy light, and their luminosity map (grayscale in the bottom panel of Figure 4) is extremely faint in this area. H15 kindly allowed us to inspect a higher-resolution version of their image, and the streak begins further north and contains more total light than in the Jee et al. (2014a) image. Without the streak, it is unclear where the galaxy luminosity peak would be located.

In summary, the literature confirms neither the gas, the galaxy luminosity, nor the lensing mass peak for this substructure, so we remove it from the ensemble analysis.

*Substructure 4:* along with Substructure 1, this is one of the two widely confirmed substructures in the system, and the H15 locations are consistent with previous work in the literature. We adopt the H15 offset. Note that this substructure carries substantially less weight than the northern substructure—at 1.6% of the total weight, it is the least weighty substructure in our literature review.

*Substructure 5:* any X-ray emission in this area is too faint to be seen in the Jee et al. (2014a) panel of Figure 4. The less highly processed X-ray image of Markevitch et al. (2005) shows what is possibly a local maximum at

this location, but it is difficult to argue that it represents a separately identifiable gas concentration. Furthermore, the visible-light peak in the H15 panel clearly consists of a single galaxy. The Jee et al. (2014a) and Clowe et al. (2012) mass contours do extend into this general area, but the H15 lensing peak lies about 100 kpc from the “spine” of those extensions. Lacking a clear association of gas, galaxy, and DM peaks, we recommend removing this putative substructure from the ensemble analysis.

### 3.4. 1E0657-56 (the Bullet Cluster)

Both substructures in this system are highly weighted in the H15 analysis: the eastern (main) subcluster ranks fourth with 6.1% of the total weight, and the western (bullet) subcluster ranks ninth with 3.8% of the total weight. These weights reflect how well the gas and galaxies are separated in this system, clearly establishing the baseline to which the galaxy-DM separation must be compared. This cluster has been extensively studied with lensing, beginning with the weak lensing analysis of Clowe et al. (2004), who used imaging from the Very Large Telescope, with two bands (*B* and *I*) for color selection of source galaxies. Another weak lensing analysis, Clowe et al. (2006), is based on a wide array of independent data: *BVR* imaging from the ESO 2.2m telescope, *BVR* imaging from the Magellan 6.5m telescope, and F606W imaging from HST/ACS, plus F435W and F814W imaging on the western subcluster. Bradač et al. (2009) used that data plus additional HST data to produce a combined strong and weak lensing analysis. More recently, Paraficz et al. (2016) produced a strong-lensing mass map using 14 multiply-imaged systems.

We show the Bradač et al. (2009) mass map (Figure 5) because it gives the reader a sense of both weak and strong lensing smoothing scales. Most of the area shown is constrained only by weak lensing, so the lower contours illustrate the smoothing and noise typical of weak lensing, while strong lensing guides some of the details in the higher contour levels. We stress that regardless of the specific reconstruction technique, all the above-cited analyses are in good agreement, and none show a displacement between mass and galaxy light in either substructure.

*East:* the H15 lensing contours place the mass about 130 kpc northwest of its position in the above-cited lensing analyses. Given the agreement among the above-cited sources, their strong exclusion of the H15 position (for example, the H15 position is well outside the Clowe et al. (2006) 99.7% confidence interval), and their advantages in data quality (such as multiple bands for source selection), we argue that the H15 position is not credible. However, it would be misleading to use the consensus lensing position with the H15 light position. This is because H15 split the light into two separate peaks and chose the lesser one because of its proximity to their lensing peak. When the mass and light are smoothed on similar scales as in Clowe et al. (2004), there is no discernible difference between the mass and light positions. We therefore adopt an offset of zero.

*West:* Clowe et al. (2004), Clowe et al. (2006), Bradač et al. (2009), and Paraficz et al. (2016) all disagree with H15 and agree with each other in placing the mass much closer to the light. The H15 position is well outside the Clowe et al. (2006) 99.7% confidence interval and outside

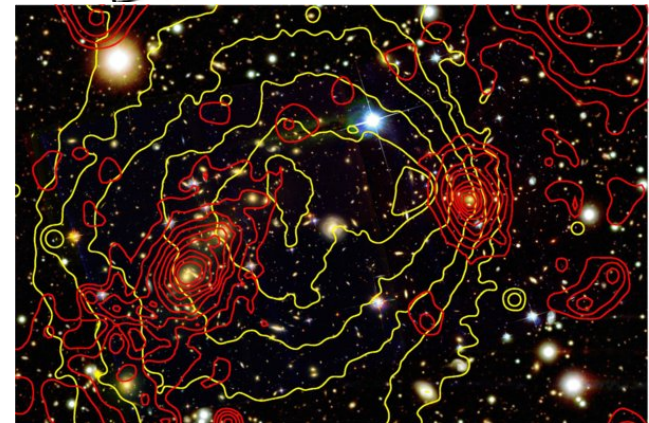
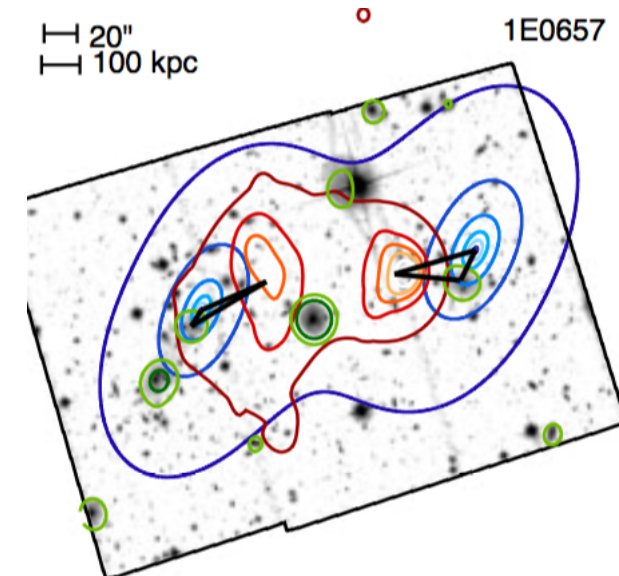


FIG. 5.— *Top*: View of the Bullet Cluster from H15. *Bottom*: maps from the more detailed analysis of Bradač et al. (2009), with mass contours from strong and weak lensing in red, and X-ray in yellow. The H15 lensing position for the western subcluster, putting the mass ahead of the galaxies, is highly excluded based on this more detailed analysis.

most of the contours in the Bradač et al. (2009) panel shown in Figure 5. Furthermore, Randall et al. (2008) explicitly analyzed the offset between galaxy and mass centroids and found the mass to be  $25 \pm 29$  to the east (for comparison, the H15 offset is just over 100 kpc to the northwest). We adopt the Randall et al. (2008) offset.

Each of these updated lensing offsets must be corrected for the gas mass contribution as described at the start of this section. This is the system least likely to need such a correction, because the lensing contours are so clearly separated from the bulk of the gas. Nevertheless, to avoid any possible bias toward SIDM we apply the mean H15 correction to each substructure. This correction leads to a final offset of  $\delta_{SI} = -4.3$  kpc in the East, and 21 kpc in the West.

### 3.5. MACS J2243.3-0935

Both subclusters in this system have substantial weight (4.9% for the east and 3.4% for the west), so we treat them together. The bottom panel in Figure 6 is from von der Linden et al. (2014), who performed a careful weak lensing analysis supported by 10 bands of photometry. In addition, Schirmer et al. (2011) analyzed a larger field in-

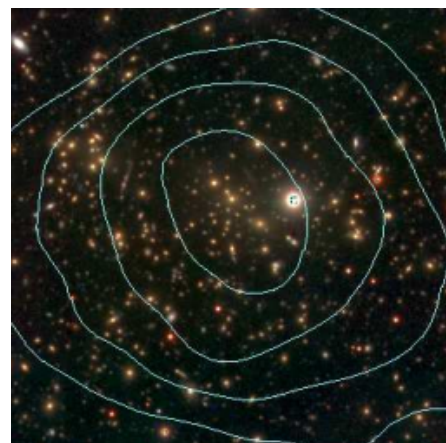
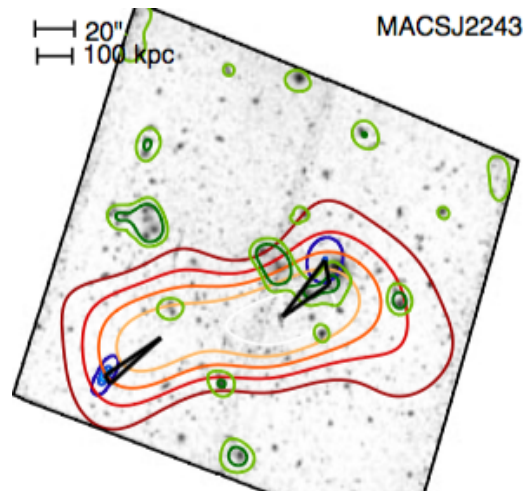


FIG. 6.— *Top*: View of MACS J2243 from H15. *Bottom*: mass contours from von der Linden et al. (2014).

cluding this system, using five-band CFHT/Megaprime imaging in good seeing. They used photometric redshifts to support source selection and member galaxy identification, and further used 190 spectroscopic redshifts to finely calibrate the photometry and obtain  $\sim 0.03$  rms redshift uncertainty. Their maps cover a much broader field at lower resolution and so are not presented here, but they confirm the von der Linden et al. (2014) picture of a single smooth, round, high S/N mass concentration centered on the galaxy concentration that appears at the center of the bottom panel of Figure 6.

The top and bottom panels of Figure 6 look rather different at first, so we advise the reader to focus first on the bright star that dominates the bottom panel. This star is also the brightest (most black) object in the upper panel, but there much of it is obscured by the blue, green, and red contours that run over it. There are two dense concentrations of galaxies, one immediately to the left (east) of this star and the other farther east. These galaxy concentrations, with heavy green contours in the H15 map, are useful points of reference when comparing the maps, but in fact neither is used by H15 as a substructure. We consider the H15 substructures individually below.

*East*: the triangle representing this substructure is seen at the lower left of the H15 image. However, there is no convincing concentration of galaxies at this position in either panel of Figure 6, nor in Schirmer et al. (2011).

Furthermore, neither von der Linden et al. (2014) nor Schirmer et al. (2011) find a lensing peak here. The absence of confirmation in more extensive data sets suggests that the H15 lensing peak is spurious. We omit this substructure from the remaining analysis.

*West:* the color image from von der Linden et al. (2014) demonstrates that the H15 luminosity peak just south of the bright star cannot be due to *galaxy* luminosity. Although H15 implemented an algorithm for removing stars before smoothing the visible light distribution, the most plausible explanation for this H15 luminosity peak is residual light from the exceptionally bright star. The green contours to the east of the bright star in the H15 panel represent a more valid galaxy luminosity position. This yields  $\delta_{SI} \approx 0$  because the galaxy-lensing offset is perpendicular to the galaxy-gas offset. The following paragraph contains more details for those with a special interest; most readers are encouraged to skip to the next subsection.

For completeness, we note that the lensing maps also disagree: the von der Linden et al. (2014) lensing map is clearly centered on the galaxies rather than on the blue H15 contour above the bright star. The von der Linden et al. (2014) map (confirmed at lower resolution by Schirmer et al. 2011) suggests that the offset between lensing and galaxy luminosity is approximately zero. In other words, with the correct luminosity position the offset is roughly zero regardless of the lensing map we adopt. The associated uncertainty is difficult to quantify from the information in von der Linden et al. (2014) and Schirmer et al. (2011), but the default H15 value of 60 kpc is a reasonable estimate. The gas mass correction is small compared to this uncertainty, but we apply it nevertheless to avoid bias in the ensemble. This yields  $\delta_{SI} = -4.3$  kpc after gas mass correction.

### 3.6. ZwCl 1358+62 (East)

Zitrin et al. (2011) performed a strong-lensing analysis of this cluster using deep six-band HST/ACS imaging. They found 23 images of eight different sources to support the construction of a mass model. The resulting critical curves are shown on top of a color ACS image in Figure 3 of Zitrin et al. (2011), repeated here as the bottom panel of Figure 7. The H15 panel shows X-ray contours strongly peaked on the BCG; this system also has a beautiful low surface brightness X-ray tail, not visible here, extending along with the galaxies to the south-southeast.<sup>8</sup> This strongly suggests a merger axis along a south-southeast direction. The Zitrin et al. (2011) strong-lensing mass reconstruction matches the mass distribution one would expect in this situation: elongated toward the south and with a secondary peak corresponding to the southern galaxies. In this context, the H15 weak-lensing finding of a large mass to the east, and none to the south, is difficult to explain.

The putative H15 mass is just off the eastern edge of the Zitrin et al. (2011) map, so there remains some possibility that the H15 mass peak is real. If so, there is essentially no associated gas peak. The X-ray tail has nearly uniform (low) surface brightness, but H15 apparently identified a local maximum and automatically

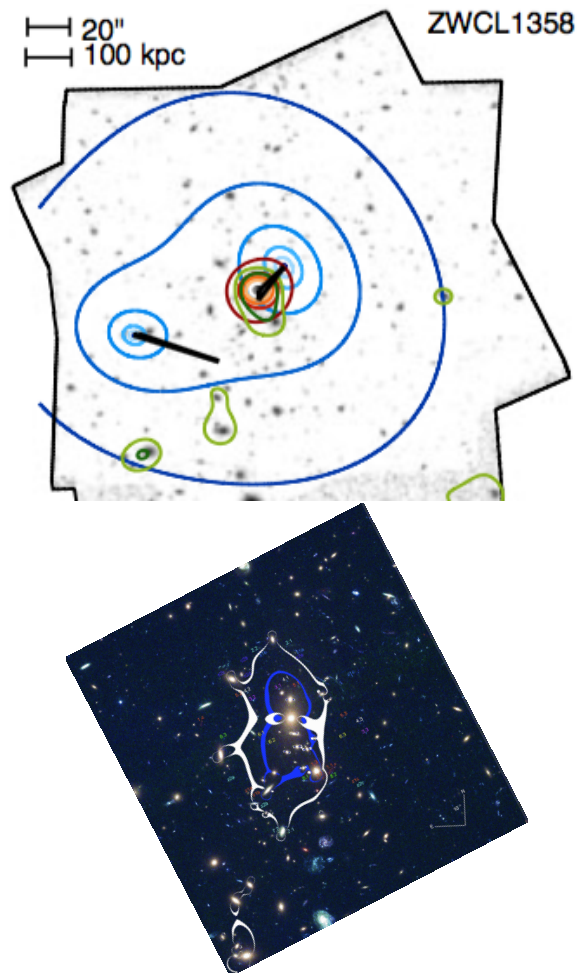


FIG. 7.— *Top:* View of ZwCl 1358 from H15. *Bottom:* lensing critical curves from Zitrin et al. (2011), showing a secondary mass peak to the south rather than to the east as shown by H15.

matched it to a peak in their mass map much further to the east. There is no plausible connection between the X-ray tail and this putative substructure in the east, as the X-ray morphology indicates a merger along an axis from the south-southeast to the north-northwest. Finally, the associated luminosity peak is not convincing either, consisting of one or two galaxies. We recommend omitting this substructure from the sample.

Observant readers may notice that the Zitrin et al. (2011) and H15 results also disagree in the main part of the cluster, near the X-ray peak. We do not examine this further because this substructure carries only 0.006% of the total weight of the sample due to the small offset between X-rays and galaxies. Also, readers wishing to search the literature on this cluster should be aware that it has several names, including but not limited to ZwCl 1358.1+6245, MS 1358.4+6245, MACS J1359.8+6231, and RXC J1359.8+6231.

### 3.7. MACS J0025.4-1222 (West)

Figure 8 compares the H15 map with that of Bradač et al. (2008), who used strong and weak lensing supported by deep three-band HST and five-band Subaru imaging. Here we are concerned only with the western substructure, on the right of each panel. The Bradač et al. (2008) mass peak (red contours) matches the posi-

<sup>8</sup> See the H15 press release image at [http://chandra.harvard.edu/photo/2015/dark/dark\\_zwcl1358.jpg](http://chandra.harvard.edu/photo/2015/dark/dark_zwcl1358.jpg).



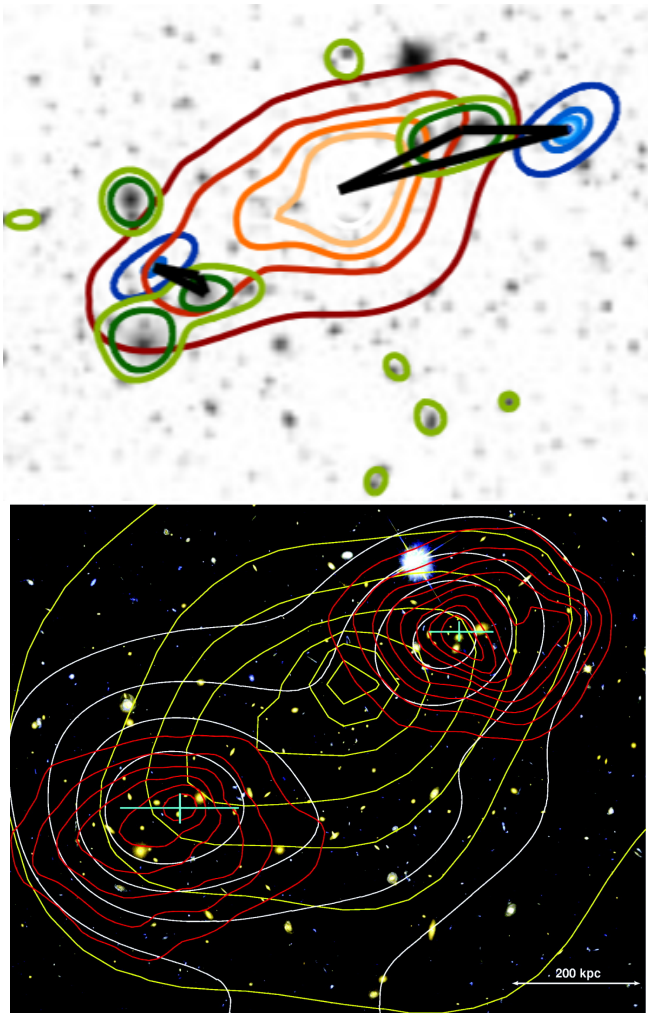


FIG. 8.— *Top*: View of MACS J0025 from H15. *Bottom*: lensing (red), X-ray (yellow), and *I*-band light (white) contours from Bradač et al. (2008). Crosses show  $1\sigma$  uncertainties on the mass positions.

tion of the luminosity contours in either panel, but not the H15 mass contours. In fact, the cyan cross in the Bradač et al. (2008) panel gives the  $1\sigma$  error bar on the mass position, showing that the H15 position is excluded at about the  $3\sigma$  level. However, Bradač et al. (2008) still find the mass to be slightly ahead of the galaxies, in large part because their galaxy position is a bit further back than the H15 position.

According to Table 2 of Bradač et al. (2008), the galaxy-mass offset is  $-4.4$  arcsec ( $-29$  kpc). With the mean H15 correction for gas mass, the final value for  $\delta_{SI}$  is  $-33$  kpc. This is a substantial change from the H15 value of  $-151$  kpc.

A recent strong lensing analysis (Cibirka et al. 2018) lends further support to the Bradač et al. (2008) results. This is the only substructure in our review where strong lensing is the major factor in determining an offset, so it is worth remarking that strong and weak lensing may correctly yield different positions if the region of highest surface mass density (probed by strong lensing) is not centered on the larger region of lower surface mass density (probed by weak lensing). In fact, SIDM simulations (Robertson et al. 2017; Kim et al. 2016; Kahlhoefer et al. 2014) show a low-density bridge forming between

the two peaks after first pericenter in a bimodal merger. This shifts the centroid but not the peak, which stays with the galaxies. Thus, a high-confidence weak lensing position is in principle preferable to a strong lensing position when probing SIDM. However, the outermost Bradač et al. (2008) contours are indeed driven by (multi-band) weak lensing, and the H15 (single-band) weak lensing position is still 110 kpc from their geometric center. Furthermore, the outer Bradač et al. (2008) contours extend in a direction opposite to that expected from the bridge argument. We thus do not find the H15 position to be supported by the bridge argument. In general, strong+weak lensing position potentially disfavor SIDM by missing possible bridge effects, so we use the Bradač et al. (2008) position to build the case that we need not make analysis choices favorable to SIDM to show that the H15 upper limits on SIDM must be revised substantially upward. However, one could also argue the opposite because the weak lensing contours extend in the “wrong” direction. For that reason, in Section 4 we assess the impact of this particular choice on the final result; it is small.

### 3.8. ACTCL J0102-4915 (*El Gordo*, *North*)

Figure 9 compares the H15 analysis with that of Jee et al. (2014b), who used four-band imaging in conjunction with the photometric redshift catalog of Menanteau et al. (2012) and 89 spectroscopic redshifts (Sifón et al. 2013) to obtain clean background source selection—a particularly important issue when the lens is itself at fairly high redshift ( $z = 0.87$ ). Jee et al. (2014b) found two mass concentrations roughly coincident with the northwest and southeast galaxy concentrations, and found no other mass concentrations in the area. H15 differ starkly in finding a mass concentration not at the northwest galaxy location, but  $\sim 700$  kpc away. The H15 location is remarkably coincident with the gap between detectors in the Advanced Camera for Surveys (ACS) data used by H15. We suggest that this is a spurious lensing peak related to the difficulty of cleaning data in or near the gap. We find further support for this suggestion in the strong lensing analysis of Zitrin et al. (2013), whose critical curves are consistent with the mass distribution of Jee et al. (2014b) but not that of H15.

Other aspects of the northern H15 substructure are problematic as well. The H15 galaxy position does not look like a galaxy overdensity in color images, and even the H15 figure panel lacks green contours at this location (the middle vertex of the triangle). Furthermore, the H15 triangle suggests a southwest-northeast merger axis, but an overwhelming variety of other evidence (all of the above-cited papers plus the radio relics presented in Lindner et al. 2014) supports a southeast-northwest merger axis; nowhere in the extensive literature on *El Gordo* is there any evidence for a southwest-northeast merger axis.

In summary, H15 have incorrectly characterized the northern substructure. We may be able to infer  $\delta_{SI}$  from Jee et al. (2014b) and/or Zitrin et al. (2013). However, there is no gas peak associated with the northwest subcluster. The detailed X-ray map of Menanteau et al. (2012) shows a large region of tenuous gas, but no identifiable peak. In this situation, even a peak-agnostic algorithm such as a centroid would have a very large asso-

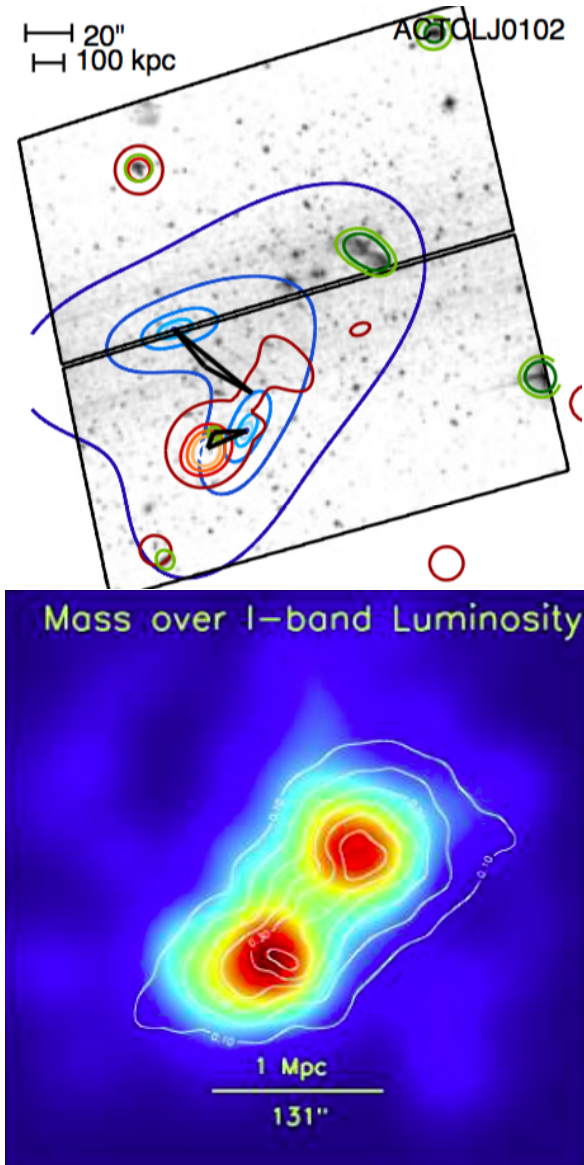


FIG. 9.— *Top*: H15 analysis of ACTCL J0102 (El Gordo). *Bottom*: lensing contours (white) and galaxy luminosity density (colormap) from Jee et al. (2014b). There is severe disagreement over the location of the northern lensing peak. The Jee et al. (2014b) location is coincident with the galaxies, while the H15 location appears to be an artifact of the ACS chip gap.

ciated uncertainty, implying that this substructure would have little influence on the ensemble. Therefore, we recommend omitting this substructure from the ensemble.

### 3.9. MACS J0417.5-1154 (North)

von der Linden et al. (2014) performed a weak lensing analysis of this cluster using three-band Subaru imaging. Their lensing map has rather low resolution and so is not presented here, but it does show the same southeast-northwest axis as the H15 lensing map (Figure 10). The galaxy distribution and X-ray morphology follow the same axis, so there is no reason to doubt the H15 lensing map.

Nevertheless, this substructure is worth discussing to illustrate some ambiguities facing next-generation analyses of this sort. First, as suggested by the H15 X-ray contours, the X-ray morphology (Mann & Ebeling 2012)

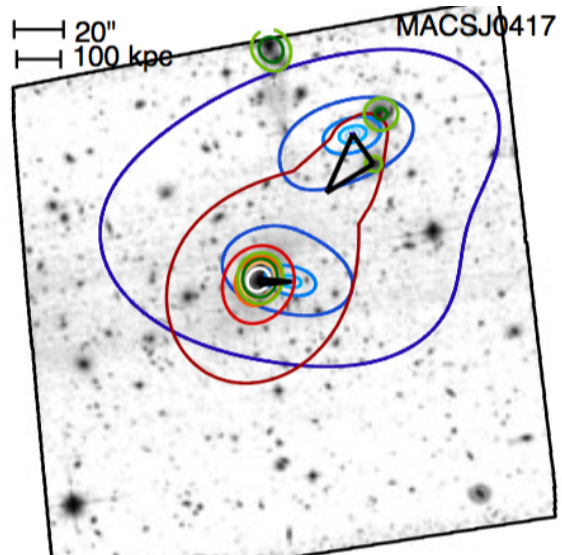


FIG. 10.— H15 analysis of MACS J0417. Only the northern subcluster is highly weighted and considered here. The X-ray morphology there consists of a long ridge rather than a peak. The luminosity peak at the top is a star and should be disregarded.

shows a long ridge to the northwest with no peak other than the main peak identified with the southern subcluster. H15 presumably identified a minor local maximum as the subcluster gas location, but this is a somewhat arbitrary location along a long smooth ridge. Without a clear X-ray peak along this ridge, there is great uncertainty in the galaxy-gas vector and therefore in the weight this substructure should receive as well as in the projection of the DM-galaxy vector onto the galaxy-gas vector. Second, the H15 DM peak appears midway between two luminosity peaks. The H15 matching algorithm chose the luminosity peak nearer the putative gas peak, yielding  $\delta_{SI} = 2$  kpc after projection onto the galaxy-gas vector). Automatically matching the nearest peak may introduce a bias: if the brighter luminosity peak had been adopted, this substructure would have different implications for SIDM, with  $\delta_{SI} \approx 50$  kpc over a longer ( $\sim 200$  kpc) galaxy-gas baseline providing a great deal of weight. Or, with more smoothing of the light, the luminosity location would be intermediate and the implication for SIDM would be intermediate. This exposes the need to develop methods less sensitive to smoothing scale, or at least an objective way to optimize the smoothing scale in each system.

### 3.10. ZwCl 1234+2916 (West)

This cluster illustrates the level of agreement we would expect for independent investigations using overlapping data. Figure 11 compares the H15 analysis with that of Dahle et al. (2013), who used two-band VLT imaging as well as the extremely deep ACS imaging in a third band (the data used by H15). The Dahle et al. (2013) lensing contours (in red) agree with H15 in showing each mass concentrations slightly to the north and, in the east-west direction, slightly closer to the center of the system compared to the corresponding galaxies. Here we are concerned with the western substructure. Although H15 put the mass concentration slightly farther north than do Dahle et al. (2013), this displacement is nearly perpendicular to the merger axis and so has little effect on  $\delta_{SI}$ .

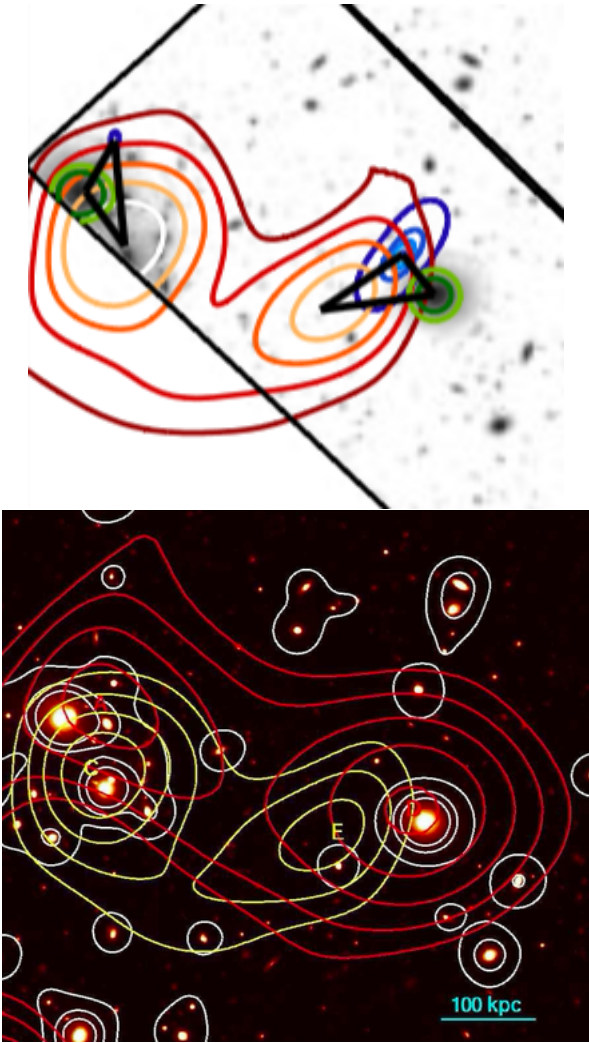


FIG. 11.— *Top*: H15 analysis of ZwCl 1234. *Bottom*: lensing (red), galaxy (white), and X-ray (yellow) contours from Dahle et al. (2013).

Dahle et al. (2013) do not list a value of  $\delta_{SI}$ , but measurements of their map yield  $\approx 10$  kpc, close to the H15 value of 28 kpc. Although the agreement is not perfect, this level of variation is to be expected in independent analyses. We retain the H15 offset.

### 3.11. Summary

Table 1 summarizes the updates we recommend after reviewing the best available evidence from the literature. In four cases the literature is consistent with the offset ( $\delta_{SI}$ ) measured by H15; in five cases there is compelling evidence that the offset differs from that of H15; and in seven cases the H15 substructure either does not exist or does not support a clear association between a gas peak, a mass peak, and a galaxy peak. Although few of the H15 offsets are retained, this set of changes is the minimum necessary to bring the H15 offset catalog in line with the literature. In the next section we quantify the impact of these changes on the dark matter inference.

## 4. DARK MATTER INFERENCE

We begin with a brief recap of the H15 prescription for inferring  $\sigma_{DM}/m$  from the offset catalog. H15 approximate the likelihood for each  $\beta_i$  as a Gaussian, as

TABLE 1  
CLUSTER WEIGHTS AND GALAXY-DM OFFSETS

Weight (%)	$\delta_{SI}$ (kpc)		Name	$\S$
	H15	Literature <sup>a</sup>		
16.7	66	Omit (M11)	Abell 2744 (west)	3.1
15.0	-19	80 (D13)	DLSCl J0916 (south)	3.2
10.1	36	No change	Abell 520-1	3.3
6.1	40	-4 (B09)	Bullet (east)	3.4
4.9	4	Omit (L14, S11)	MACS J2243 (east)	3.5
4.7	-7	Omit (Z11)	ZwCl 1358 (east)	3.6
4.7	81	Omit (J14a)	Abell 520-2	3.3
4.1	-151	-33 (B08)	MACS J0025 (west)	3.7
3.8	-32	21 (B09,R08)	Bullet (west)	3.4
3.4	-26	-4 (L14)	MACS J2243 (west)	3.5
2.9	22	Omit (J14a)	Abell 520-5	3.3
2.4	-150	Omit (J14b)	ACTCL J0102 (north)	3.8
2.1	2	No change	MACS J0417 (north)	3.9
1.8	28	No change	ZwCl 1234 (west)	3.10
1.7	84	Omit (C12,J14a)	Abell 520-3	3.3
1.6	-22	No change	Abell 520-4	3.3

<sup>a</sup>References: B08 (Bradač et al. 2008); B09 (Bradač et al. 2009); C12 (Clowe et al. 2012); D13 (Dawson 2013); J14a (Jee et al. 2014a); J14b (Jee et al. 2014b); L14 (von der Linden et al. 2014); M11 (Merten et al. 2011); R08 (Randall et al. 2008); S11 (Schirmer et al. 2011); Z11 (Zitrin et al. 2011).

described in Section 2. They multiply these likelihoods to find a likelihood for  $\langle\beta\rangle$  and then transform this into a likelihood for  $\sigma_{DM}/m$  according to the relation  $\sigma_{DM}/m = -\sigma_* \ln(1 - \beta)$ , where  $\sigma_*$  is the characteristic cross-section (per unit mass) at which a halo becomes optically thick. They choose a central value of  $\sigma_* = 6.5 \text{ cm}^2/\text{g}$  and “analytically marginalize” over the range  $3.5 \leq \sigma_* \leq 9.5$  by quadrature addition to the second moments of the  $\sigma_{DM}/m$  likelihood.

We prefer to marginalize numerically so that any non-Gaussian features can be preserved. We create a grid of models in the  $(\sigma_{DM}/m, \sigma_*)$  parameter space, covering the region  $(0 - 5, 3.5 - 9.5)$ . For each point in the grid we multiply the  $\beta_i$  likelihoods as determined by the H15 prescription. We then marginalize over the  $\sigma_*$  axis to obtain a likelihood.

Figure 12 shows a digitized version of H15 Figure 4 (gray), along with the result of our marginalization procedure (cyan) using their offsets (as well as their nominal 60 kpc uncertainty on each offset). The two results differ only slightly, with peak locations shifted by  $\approx 0.25 \text{ cm}^2/\text{g}$ , or  $\approx 0.6$  times the uncertainty given by H15. Correcting the most highly weighted offsets based on our literature review, as listed in Table 1, then yields the blue curve. Using *only* the offsets from the vetted systems yields the black curve. The black peak is shifted from the gray by about twice the uncertainty given by H15, still not highly significant. For context, the red curve shows the shift that can result from an even simpler variation on the H15 analysis: adopting the individual offset uncertainties displayed in their Figure S2 (rather than the uniform 60 kpc uncertainty they adopted in their analysis) while retaining their offset measurements. This also yields a  $\approx 2\sigma$  shift in the same direction.

Models with  $\sigma_{DM}/m < 0$  are not physical. To constrain physical models, we apply a prior that is uniform for  $\sigma_{DM}/m \geq 0$  and zero otherwise. Note that this will have little effect when using, say, the red likelihood in Figure 12, because this likelihood already nearly vanishes for  $\sigma_{DM}/m < 0$ . Conversely, the prior will have a substantial effect when using the gray likelihood, which peaks in negative territory. In the following, we show

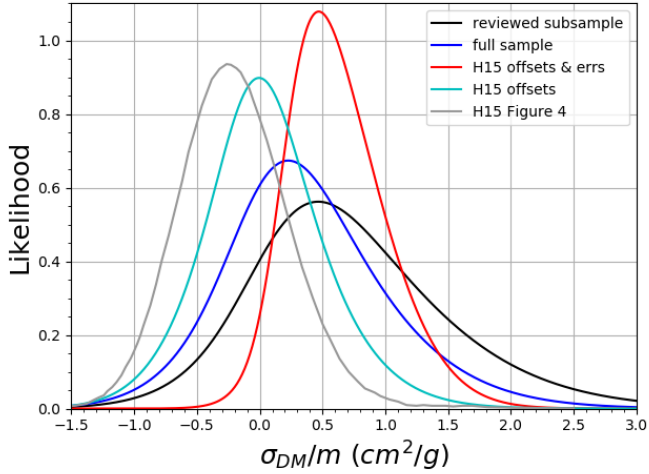


FIG. 12.— Likelihoods, normalized to unit area, for variations on the cross-section analysis. Our marginalization using the H15 offsets and their adopted 60 kpc uncertainty on each offset (cyan) agrees with the H15 result (gray) to well within  $1\sigma$ . The blue curve incorporates corrections to the offsets based on our literature review of the most highly weighted substructures; the black curve is based *only* on these reviewed substructures; and the red curve uses the H15 offsets *and* their individualized uncertainties as displayed in H15 Figure S2.

results with and without the prior for completeness.

After optional application of the prior, we integrate each posterior into a cumulative distribution function (CDF), which allows the reader to quickly read an upper limit at any desired confidence level. Figure 13 shows CDFs with (solid) and without (dashed) the physical prior, with color coding to match Figure 12. As an example of how to read this figure, the dashed gray (H15) curve in Figure 13 indicates 70% confidence that  $\sigma_{\text{DM}}/m < 0$  and 95% confidence that  $\sigma_{\text{DM}}/m < 0.5 \text{ cm}^2/\text{g}$  with no prior, but the solid curve indicates substantially less confidence in those limits after applying the prior. In contrast, the red solid and dashed curves in Figure 13 are nearly identical; this means that the constraint using the H15 offsets and uncertainties is nearly unaffected by the prior, as predicted in the previous paragraph. The 95% confidence limits from our reviewed subsample, or the full (corrected) sample, are only marginally affected by the prior.

Regardless of the prior, Figure 13 reveals a dramatic relaxation of upper limits when using the best available information about each cluster:  $\sigma_{\text{DM}}/m < 1.71 \text{ cm}^2/\text{g}$  at 95% confidence for the full sample, or  $2.27 \text{ cm}^2/\text{g}$  for the reviewed subsample. This is driven by the data, not the prior: the upper limits change by  $0.15 \text{ cm}^2/\text{g}$  or less when dropping the prior for these data. On the other hand, the strict upper limit quoted by H15 for their data is possible *only if* the physical prior is discarded.

So far our discussion has considered any (nonnegative) value of  $\sigma_{\text{DM}}/m$  to be equally likely *a priori*. If instead we treat  $\sigma_{\text{DM}}/m = 0$  (cold dark matter) as a null hypothesis, it is clear that all likelihoods in Figure 12 are consistent with this hypothesis.

We tested the sensitivity of the analysis to additional variations. As a reminder, our default analysis follows H15 in assigning 60 kpc uncertainty to each value of  $\delta_{SI}$ —not because we endorse this proce-

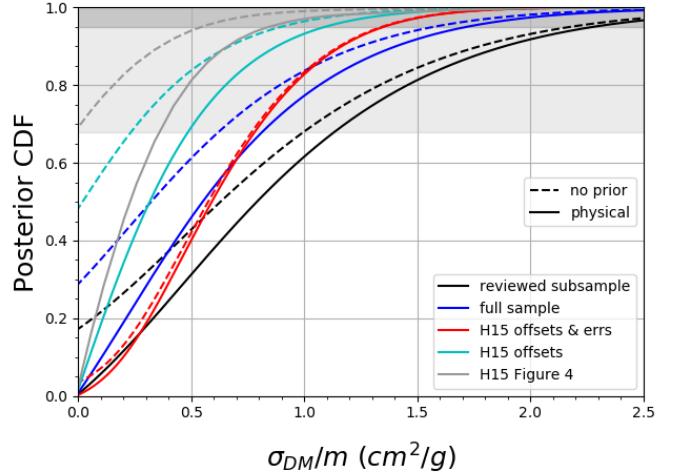


FIG. 13.— Constraints on  $\sigma_{\text{DM}}/m$  with (solid) and without (dashed) the physical prior  $\sigma_{\text{DM}}/m \geq 0$ . All variations on the H15 analysis lead to substantially relaxed upper limits. The reviewed samples lead to 95% upper limits of  $\approx 1 - 2 \text{ cm}^2/\text{g}$  regardless of prior. The prior becomes more important when interpreting the H15 PDF, because most of its area is at negative cross section. Color codes are the same as in Figure 12.

dure, but to demonstrate that a *minimal* set of changes to the H15 offsets and procedures yields substantially looser constraints. In one variation, we used the uncertainties displayed by H15 in their Figure S2 with our literature-based offsets. In a second variation, we inserted literature-based uncertainties where explicitly available, i.e. for the Bullet Cluster West (Randall et al. 2008,  $25 \pm 29 \text{ kpc}$ ). In a third variation, we explored the sensitivity to gas mass correction by adding the mean 4.3 kpc correction back to each value of  $\delta_{SI}$ . In all cases the constraint shifted by substantially less than the difference between the black and blue curves in Figure 13.

We also tested the sensitivity to individual updates. The omission of Abell 2744 West lowered the most likely value of  $\sigma_{\text{DM}}/m$  by  $0.19 \text{ cm}^2/\text{g}$ , and the update to DLSCL J0916 South raised it by  $0.24 \text{ cm}^2/\text{g}$ ; other individual updates had at most half this effect. This suggests that our scheme for estimating the weight of each subcluster in the ensemble analysis is effective, and that the most important subclusters have indeed been reviewed. Note that the size of the proposed change matters as well as the weight of the subcluster: omitting the remarkably large negative offset of ACTCL J0102 (based on a spurious lensing position) had the third largest effect (a  $+0.12 \text{ cm}^2/\text{g}$  shift), outstripping smaller adjustments to more highly weighted subclusters. Updating MACS J0025 West from  $-151$  to  $-33 \text{ kpc}$  had the fourth-largest effect, a  $+0.11 \text{ cm}^2/\text{g}$  shift. Thus, if one favors weak lensing contours as discussed in §3.7 and uses a slightly more negative offset for this substructure, the ensemble result would be lowered by a fraction of  $0.11 \text{ cm}^2/\text{g}$ .

To summarize this section, when using the H15 offsets we find a most likely value of  $\sigma_{\text{DM}}/m$  that is slightly higher than, but consistent with, the H15 value. After updating the most highly weighted offsets according to our literature review, the most likely value shifts further upward to  $+0.23 \text{ cm}^2/\text{g}$  (blue curve in Figure 12). The corresponding upper limit (at 95% confidence) is  $1.71 \text{ cm}^2/\text{g}$  if one adopts a physical prior (as we recommend),

or  $1.57 \text{ cm}^2/\text{g}$  if one does not. These limits are substantially higher than found by H15, and increase further by about  $0.5 \text{ cm}^2/\text{g}$  if one uses *only* the reviewed subsample of highly weighted subclusters. Our higher upper limits are robust against many variations in the analysis.

## 5. SUMMARY AND DISCUSSION

Adopting the H15 methodology but with corrections to their offsets based on the best available evidence in the literature and marginalizing only over physical models, we find a 95% confidence upper limit on  $\sigma_{\text{DM}}/m$  of  $\lesssim 2 \text{ cm}^2/\text{g}$ , depending on whether one uses the high-quality subsample or the full sample. In other words, the H15 methodology does not yet support constraints tighter than the  $1.25 \text{ cm}^2/\text{g}$  at 68% confidence quoted by Randall et al. (2008). In this discussion we first defend the literature-review approach that led to this conclusion. Then, we explain why the H15 sample selection should lead readers to use even the revised constraints with caution. Finally, we discuss future prospects.

We predict two types of concerns readers may have with our approach:

- **Bias:** was evidence from the literature applied consistently without regard to the effect on the final result? It is impossible to remain ignorant of the potential impact of a change in the offset when reviewing the H15 star-gas-DM geometry, because the geometry is so simple: if DM is self-interacting then it should be bracketed by the stars and the gas. We have attempted to minimize this concern by systematically examining the highest-weight substructures rather than the most negative or most suspect offsets. As *post facto* evidence that our review was not biased, we note that of the seven H15 substructures we omitted, five had positive offsets in H15, and only two had negative offsets. By itself, this should bring  $\sigma_{\text{DM}}/m$  down rather than up, barring complications such as the differing weights and sizes of the offsets. Of the changes to  $\delta_{SI}$  that we recommend, the majority do go in the direction of lifting  $\sigma_{\text{DM}}/m$  from its H15 value, but the literature on these systems is so compelling that it speaks for itself.
- **Inhomogeneity:** the H15 catalog was produced in a mostly uniform way and uses only ACS data for photometry and lensing, but our corrections are based on a variety of data and analyses from the literature. While uniformity is a laudable goal, we do not believe it overrides the compelling evidence in the literature. Indeed, we believe the concern for uniformity is a major reason some of the H15 offsets are in error: single-band photometry is not sufficient to adequately characterize the mass and luminosity distribution of these systems.

These arguments suggest that any ill effects of bias and inhomogeneity are likely to be smaller than the beneficial effect of using more correct offsets.

We now turn to concerns about sample selection. The equation used by H15 to relate  $\beta$  to  $\sigma_{\text{DM}}/m$  was developed assuming only small ( $\lesssim 30 \text{ kpc}$ ) displacements between DM, galaxies and gas; Harvey et al. (2014) clearly shows how the analogy between galaxy and gas restoring

forces (and hence the inferred drag force) breaks down quickly beyond 30 kpc displacements. Yet, many of the H15 offsets are very far outside this regime. Figure S2 of H15 readily shows that only five of the 72 substructures have both  $\delta_{SI}$  and  $\delta_{SG}$  within 30 kpc. Our updates have modestly reduced the spread of  $\delta_{SI}$  values, but many violations of this approximation remain. In fact, the ensemble result is *driven* by substructures that violate the approximation, because the weight of each substructure is approximately proportional to  $\delta_{SG}^2$  (Equation 3).

The analogy between gas and self-interacting DM can break in other ways as well, for example if the gas is completely stripped at pericenter crossing. The analogy also breaks after the drag force (if any) subsides, for example well after pericenter as the subcluster travels to regions of lower and lower density. Subsidence of the drag force allows the gas and galaxies to each fall back to, and *through*, the DM. Recent SIDM simulations by Kim et al. (2016) clearly show the sign of the DM-galaxy offset changing as this happens. Separately, it has also been seen with gas in an effect known as the ram pressure slingshot: after ram pressure pulls the gas back from the center of the subcluster potential, gravity slings it forward (Markevitch & Vikhlinin 2007; Mathis et al. 2005; Hallman & Markevitch 2004; Ng et al. 2015). Because the maximum galaxy-DM displacement is smaller than the maximum gas-DM displacement, the two components cannot fall through the DM on the same timescale. Thus the ratio of displacements  $\beta$  cannot remain constant over time, and could even change sign at times. Averaging over a sample without regard to merger phase would then bias the inferred cross section low. We therefore suggest caution in interpreting even the revised constraints.

Although this conclusion is disappointing for current constraints, it does suggest that constraints from merging clusters could be tightened with a closer analysis of key systems including modeling the merger phase. We suggest that post-pericenter systems should be modeled with hydrodynamic simulations (e.g., Robertson et al. 2017) rather than with an analytical formalism. Other aspects of cluster infall are also potentially competitive (Kahlhoefer et al. 2015).

Cluster mergers can also be used to test SIDM effects that cannot be modeled with a drag force; as noted by Kahlhoefer et al. (2014), the drag-force model maps well to frequent interactions with low momentum transfer, as in a long-range force. Infrequent interactions with large momentum transfer (as in hard scattering), in contrast, can eject particles from the cluster and is potentially observable as a decrease in the mass-to-light ratio; Randall et al. (2008) used the Bullet Cluster to constrain these models with an upper limit of  $\sigma_{\text{DM}}/m < 0.7 \text{ cm}^2/\text{g}$  (68% confidence). This gives clusters a purpose beyond constraining the cross section at high velocity: if dark matter does interact with itself, comparing the two types of cluster constraints could point the way to a particle model of the interactions.

We close with a simple message: single-band imaging is insufficient to properly identify mass and light peaks. H15 argue that single-band imaging suffices for a large sample because errors will average out. We showed, however, that some substructures have much more weight

than others in the ensemble, and that single-band imaging enables errors on individual substructures to be quite large, up to hundreds of kpc. As a result, the errors cannot be counted on to cancel over the H15 sample.

We thank Maruša Bradač, James Bullock, Bill Forman, James Jee, Felix Kahlhoefer, Manoj Kaplinghat, and Reinout van Weeren for helpful discussions, as well

as the anonymous referee for useful feedback. We especially thank David Harvey for being completely open with his code and his data, patiently answering our questions, and reviewing a complete draft. DW and NG were supported by NSF grant 1518246. Part of this work performed under the auspices of the U.S. DOE by LLNL under Contract DE-AC52-07NA27344.

## REFERENCES

- Boylan-Kolchin, M., Bullock, J. S., & Kaplinghat, M. 2012, *MNRAS*, 422, 1203
- Bradač, M., Allen, S. W., Treu, T., Ebeling, H., Massey, R., Morris, R. G., von der Linden, A., & Applegate, D. 2008, *ApJ*, 687, 959
- Bradač, M., et al. 2009, *ApJ*, 706, 1201
- Brooks, A. 2014, *Annalen der Physik*, 526, 294
- Cibirka, N., et al. 2018, *ArXiv e-prints*
- Clowe, D., Bradač, M., Gonzalez, A. H., Markevitch, M., Randall, S. W., Jones, C., & Zaritsky, D. 2006, *ApJ*, 648, L109
- Clowe, D., Gonzalez, A., & Markevitch, M. 2004, *ApJ*, 604, 596
- Clowe, D., Markevitch, M., Bradač, M., Gonzalez, A. H., Chung, S. M., Massey, R., & Zaritsky, D. 2012, *ApJ*, 758, 128
- Cohen, T., Phalen, D. J., Pierce, A., & Zurek, K. M. 2010, *Phys. Rev. D*, 82, 056001
- Dahle, H., et al. 2013, *ApJ*, 772, 23
- Dawson, W. A. 2013, PhD thesis, University of California, Davis
- Dawson, W. A., et al. 2012, *ApJ*, 747, L42
- Elbert, O. D., Bullock, J. S., Garrison-Kimmel, S., Rocha, M., Oñorbe, J., & Peter, A. H. G. 2015, *MNRAS*, 453, 29
- Feldman, D., Kors, B., & Nath, P. 2007, *Phys. Rev. D*, 75, 023503
- Feng, J. L., & Kumar, J. 2008, *Phys. Rev. Lett.*, 101, 231301
- Hallman, E. J., & Markevitch, M. 2004, *ApJ*, 610, L81
- Harvey, D., Massey, R., Kitching, T., Taylor, A., & Tittley, E. 2015, *Science*, 347, 1462
- Harvey, D., et al. 2014, *MNRAS*, 441, 404
- Jauzac, M., et al. 2016, *MNRAS*, 463, 3876
- Jee, M. J., Hoekstra, H., Mahdavi, A., & Babul, A. 2014a, *ApJ*, 783, 78
- Jee, M. J., Hughes, J. P., Menanteau, F., Sifón, C., Mandelbaum, R., Barrientos, L. F., Infante, L., & Ng, K. Y. 2014b, *ApJ*, 785, 20
- Kahlhoefer, F., Schmidt-Hoberg, K., Frandsen, M. T., & Sarkar, S. 2014, *MNRAS*, 437, 2865
- Kahlhoefer, F., Schmidt-Hoberg, K., Kummer, J., & Sarkar, S. 2015, *MNRAS*, 452, L54
- Kaplinghat, M., Tulin, S., & Yu, H.-B. 2016, *Physical Review Letters*, 116, 041302
- Kim, S. Y., Peter, A. H. G., & Wittman, D. 2016, *ArXiv e-prints*
- Klasen, M., Pohl, M., & Sigl, G. 2015, *Progress in Particle and Nuclear Physics*, 85, 1
- Lindner, R. R., et al. 2014, *ApJ*, 786, 49
- Loeb, A., & Weiner, N. 2011, *Physical Review Letters*, 106, 171302
- Mann, A. W., & Ebeling, H. 2012, *MNRAS*, 420, 2120
- Markevitch, M., Gonzalez, A. H., Clowe, D., Vikhlinin, A., Forman, W., Jones, C., Murray, S., & Tucker, W. 2004, *ApJ*, 606, 819
- Markevitch, M., Govoni, F., Brunetti, G., & Jerius, D. 2005, *ApJ*, 627, 733
- Markevitch, M., & Vikhlinin, A. 2007, *Phys. Rep.*, 443, 1
- Mathis, H., Lavaux, G., Diego, J. M., & Silk, J. 2005, *MNRAS*, 357, 801
- Medezinski, E., Umetsu, K., Okabe, N., Nonino, M., Molnar, S., Massey, R., Dupke, R., & Merten, J. 2016, *ApJ*, 817, 24
- Menanteau, F., et al. 2012, *ApJ*, 748, 7
- Merten, J., et al. 2011, *MNRAS*, 417, 333
- Newman, A. B., Treu, T., Ellis, R. S., & Sand, D. J. 2013a, *ApJ*, 765, 25
- Newman, A. B., Treu, T., Ellis, R. S., Sand, D. J., Nipoti, C., Richard, J., & Jullo, E. 2013b, *ApJ*, 765, 24
- Ng, K. Y., Dawson, W. A., Wittman, D., Jee, M. J., Hughes, J. P., Menanteau, F., & Sifón, C. 2015, *MNRAS*, 453, 1531
- Paraficz, D., Kneib, J.-P., Richard, J., Morandi, A., Limousin, M., Jullo, E., & Martinez, J. 2016, *A&A*, 594, A121
- Peter, A. H. G., Rocha, M., Bullock, J. S., & Kaplinghat, M. 2013, *MNRAS*, 430, 105
- Randall, S. W., Markevitch, M., Clowe, D., Gonzalez, A. H., & Bradač, M. 2008, *ApJ*, 679, 1173
- Robertson, A., Massey, R., & Eke, V. 2017, *MNRAS*, 465, 569
- Rocha, M., Peter, A. H. G., Bullock, J. S., Kaplinghat, M., Garrison-Kimmel, S., Onorbe, J., & Moustakas, L. A. 2013, *MNRAS*, 430, 81
- Sand, D. J., Treu, T., Ellis, R. S., Smith, G. P., & Kneib, J.-P. 2008, *ApJ*, 674, 711
- Schirmer, M., Hildebrandt, H., Kuijken, K., & Erben, T. 2011, *A&A*, 532, A57
- Sifón, C., et al. 2013, *ApJ*, 772, 25
- von der Linden, A., et al. 2014, *MNRAS*, 439, 2
- Zavala, J., Vogelsberger, M., & Walker, M. G. 2013, *MNRAS*, 431, L20
- Zitrin, A., Broadhurst, T., Coe, D., Liesenborgs, J., Benítez, N., Rephaeli, Y., Ford, H., & Umetsu, K. 2011, *MNRAS*, 413, 1753
- Zitrin, A., Menanteau, F., Hughes, J. P., Coe, D., Barrientos, L. F., Infante, L., & Mandelbaum, R. 2013, *ApJ*, 770, L15